

Super-Resolution Algorithm for Captured Images by "All-Sky System"

Roberto Solís, Christian Quintana, Nelson Vejar, Claudia Alvarado, Joseph Rozas and Renato Zamora
Center for Research and Development in Aerospace Sciences. Chile Air Force.
Santiago, Chile

Abstract:- The atmospheric images captured by the All-Sky systems correspond to images of low visual quality, so their subsequent study is limited to the optical capabilities of the sensors with which they were captured, improving these deficiencies based on recent processing techniques of images based on super-resolution not only allows to improve the levels of the capture of transient elements related to the increase or improvement of the level of definition or quality of the images but also to recover the night sky in areas where light and atmospheric pollution only allows to detect faint light signals from stars and their different elements. The objective of this work was to develop an algorithm capable of increasing the faint electromagnetic signals captured by the sensors and that are not visible to the naked eye. This process is carried out by integrating the pixels of a given astronomical zone and applying different improvements focused on the pixels, generating a single super-resolution image, with a greater amount of data per pixel, from four low-resolution images. Being the Matlab modeling software, the main tool for developing the algorithm is achieving a 126% improvement in resolution over the original capture system.

Keywords:- Super-Resolution; All-Sky System; Pixel Integration; Transient Elements.

I. INTRODUCTION

The observation of the skies is a discipline that integrates several branches of science and technology, generating significant interest, both from the scientific community and from hobbyists. However, its progress is becoming more complex every day due to the light and atmospheric pollution present in the skies. In this context, some of the critical solutions have been the image processing techniques based on super-resolution, which are applied to the images captured by atmospheric monitoring and control systems to obtain an improvement in quality visual and spatial resolution of the final processed image, thereby increasing the detection capabilities of transient elements, such as meteorites, comets, satellites, and asteroid [1].

Super-resolution (SR) consists of a set of techniques focused on increasing the spatial resolution or quality of a digital image. That arises from the visual limitations that optical sensors have, as they cannot capture all the electromagnetic frequencies that occur in the visible

spectrum [2]. Super-resolution processes start by increasing the number of pixels in a digital image by estimating unknown pixel values, using different images or variations thereof, known as low-resolution, which, when processed by an algorithm image processing based on SR techniques, generates a final high-resolution image. SR models generated from multiple images taken sequentially by different sensors are used to capture the faint electromagnetic frequencies of the transient elements and represent variations of pixels in the data matrix of digital images [3]. High-resolution images can be generated from this model, with a high visual quality of the transient elements in astronomical images, thus enhancing atmospheric monitoring and control systems.

In research on Space Objects (SO), devices have been developed to improve the observation of the sky and objects around the Earth, as well as active and inactive satellites and space debris. [4]. And thus, have devices that capture a wide field of vision and with a higher sampling rate than the telescopes used in the most classical tasks of astronomy [5].

Trigo-Rodriguez et al. [6] since 2004 they have monitored meteoroids and meteors with the Spanish Meteor Network (SPMN), a network of four stations located in Spain equipped with All-Sky type cameras that capture high-resolution images (4096x4096 pixels) and field of vision practically complete given its lens type "fisheye".

The Croatian Meteor Network (CMN) [7], which since 2006 operates using low-cost video cameras that allows capturing at a sampling rate of 25 images per second in low resolution. This monitoring network generates images considering the maximum values of each pixel in sequences of 1500 frames (60 seconds) and, in turn, storing the frame number in which the maximum of each pixel was obtained to have temporal information on the capture.

R.J. Weryk, in 2007, developed the Southern Ontario All-Sky Meteor Camera Network [8], located in Canada and made up of five stations equipped with low-resolution video cameras (640x480 pixels). R.J. Weryk also participated in the development of the Canadian Automated Meteor Observatory (CAMO) [9] which is made up of two stations equipped with video cameras, one of which is located next to the Canadian Meteor Orbit Radar (CMOR) [10] precisely to analyze the video-radar combination.

Higher-cost telescopes, such as TAROT (Telescope à Action Rapide pour les Objets Transitoires), have been used to detect satellites and space debris [11, 12]. Initially, TAROT was an isolated telescope, but later more telescopes were added to the system creating an observation network focused on space surveillance [13]. One of TAROT's telescopes is in Chile, specifically at the La Silla Observatory, operating since 2006.

Regarding the development of hardware dedicated to the detection of space debris, the Omnidirectional Space Situational Awareness (OmniSSA) Array [14] stands out, which has three cameras that simultaneously capture the same area of the sky, with which it seeks to improve the quality of the images obtained and, in turn, improve the detections.

It is vitally important to have algorithms and methods to process the acquired data and detect SO efficiently. In this context, Gural [15] develops a series of algorithms for detecting meteors, highlighting the one implemented to work with SPMN images, which were taken considering an exposure time of 90 seconds. The algorithm above takes two consecutive images, calculates their difference, and applies a Hough transform variant to detect moving objects.

Regarding the images generated by the CMN, the software was also developed by Gural [7] and consists of a series of sequential processes that include background estimation stages, background subtraction, reconstruction of each frame from the image compressed, use of a variant of the Hough Transform and a Matched-Filter type detector. Subsequently, different improvements and updates have been implemented to the CMN system [16, 17]. In addition, new methods of meteor detection have been studied, and such as the one proposed by Filip Novoselnik [18] that by applying a horizontal spatial filter generates a binary image, then it generates clusters in the pixels of the binary image that are considered as candidates to be a meteor. Afterward, said candidates go through a verification stage that applies a vertical spatial filter to determine that the clusters found by both filters are consistent. Also, candidates that have a circular shape are discarded.

The methodology with which the images obtained by TAROT are processed [19] consists of applying morphological operations to eliminate the elements that are not of interest, such as stars. Next, the Hough Transform is used to detect the objects mobile, such as the non-geostationary satellites. Next, a method is applied to eliminate events produced by cosmic rays to reduce false positives. Finally, the remaining points in the image are extracted, which represent geostationary satellite detections.

Another of the strategies proposed for detecting objects that orbit the Earth is the one presented by Zimmer et al. [20], which uses a variant of the Radon Transform. In later works [21], results have been demonstrated using real captures obtained with a high-resolution capture system, slight field of vision, and 1 second sampling rate, specially designed to detect objects circulating in the low and medium

Earth orbits (LEO and MEO). Systems based on Matched-Filter methods have also been developed [22]. However, for their application, it is necessary to have prior information about the objects searched.

Finally, in recent years some groups of researchers have incorporated Machine Learning techniques into SO detection systems. An example of the above is a methodology composed of an image processing stage to detect suspected SO, subsequently analyzed by a trained classifier that determines if they are part of the objects of interest [23].

II. EXPERIMENTAL METHOD

The development of the algorithm design was raised from four main tasks. The first task was to establish a graphical representation of the algorithm's operation, which allows to visualize and understand the manipulation performed on the image when the algorithm processes it. The second task consisted of establishing the technical level that corresponds to the application of hardware and software required to process atmospheric photos. The third task was to define the operational status of the initial images to obtain a good result, which required knowing the scenario and its variants to establish optimal operation. The fourth and last task consisted of creating a mathematical model adjusted to the processing of atmospheric images since the images behave like numerical matrices and require functions to carry out the corrective processes.

In Fig. 1, a diagram of the system's operation is presented, from the simultaneous capture of images to the final result of an image in super-resolution condition. In the first stage, the system, with its four cameras, obtains simultaneous photos of the night sky. Then, its calibration is carried out with the superposition of images to rescue the greatest amount of data from the captures. Finally, in the third stage, the image obtained from the overlay of captures is processed in the super-resolution algorithm, and it is also digitally filtered to finally obtain a single super-resolution image of the night sky in the fourth stage of the process.

The proposed design corresponds to a super-resolution model based on the restoration and reconstruction of atmospheric images; the model considers that these images present many considered noise elements, but they correspond to transient elements that should not be eliminated. The model is in charge of rescuing pixels from the shots taken, presenting an improvement in the quality and resolution of the processed image from processes focused on improving the sensor's capabilities that captures the images. The sequence is formed to reconstruct pixels and not remove any element from the digital image. The solution proposes a logical sequence of stages that are defined below.

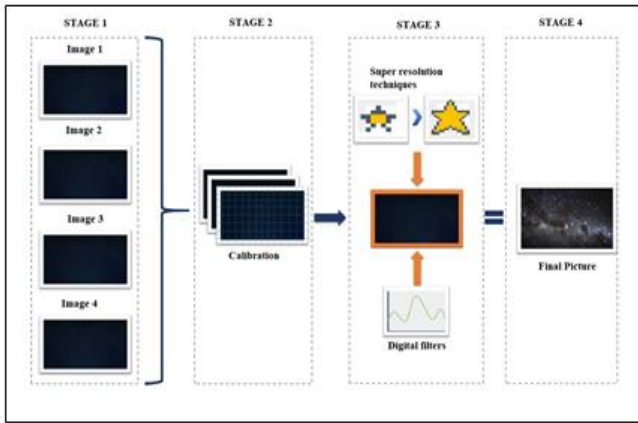


Fig. 1. Conceptual diagram of the development stages, from the captures obtained to the final result of a single super-resolution image.

A. 1st Stage

The need to have four images captured simultaneously by four different sensors was raised. This solution is born due to the electromagnetic properties of light in space, which, when interacting with the atmosphere, generates a disturbance of the oscillation of the electromagnetic wave, which causes the captured images not to represent all the elements that the scene contains. This disturbance corresponds to a wave disturbance already established for astronomical models, which can be suppressed by other sensors that capture these frequencies when they are in another position.

The proposed solution allows capturing a more significant number of pixels of the element that transits through the atmosphere, considering that the Earth's rotation is 30 km per second. The elements that pass through will be captured in millisecond segments (flashes of light per pixel). In addition, each image will come with a pixel variant, allowing greater detection by applying the super-resolution algorithm to the system to reconstruct the image segment.

The images used must reach an altitude of 500 km focal plane. For the element at a higher elevation to be detected, it has to complete the area of vision extension of the pixel by 80%. It should be noted that, by using four images from four different sensors, the resulting composite image to which the algorithm is applied allows the capture area to be reduced to a quarter. This area can be further improved by applying an optical lens over the sensor, although it decreases its angle of view.

B. 2nd Stage

Having four images of a common scenario is necessary to obtain the validated section to apply the super-resolution. This section corresponds to the matrix of pixels that the four images captured at the same time. An example of the section corresponding to this segment is shown in Fig. 2. This process is known as image registration. There are numerous techniques to carry out the proposed process, present a better result, and use fewer command lines. These are achieved, taking each valid segment in the four images that must be cut, then superimposed to generate a composite

image with a greater amount of data per pixel. Due to the electromagnetic properties of light when interacting with the atmosphere, which was pointed out earlier.

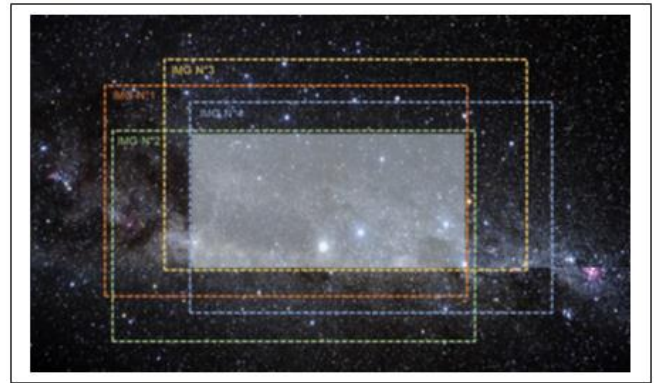


Fig. 2. Composition of the valid segment to apply super-resolution.

C. 3rd Stage

The third stage required evaluating functional techniques of super-resolution based on image reconstruction and restoration that improve atmospheric images and presenting filters that reduce noise and blur generated in the captured scene to deliver a better final result. For this, different techniques and filters were evaluated.

1) *Super-resolution technique:* This technique requires selecting the methods for the image restoration and reconstruction processes in the first stage. Interpolation was the technique that met these requirements because it does not modify the image data, does not perform transformations to the data matrix. Its function is to subsample the image signal, being the most suitable to apply in astronomical images.

To select the type of linear interpolation, you must first know that not all interpolation methods are recognized as Super-resolution techniques; only models that use polynomials as carriers are valid. In this case, only the Bilinear, Bicubic, and Lanczos3 interpolation correspond to this process. Next, a selection evaluation was carried out, which focused on measuring the initial resolution, the final resolution, the average matrix, the processing time, the structural similarity index, and the signal-to-noise portion. Finally, this process was carried out using a low-resolution image of the night sky, applying interpolation and comparing it with the initial image to define and support the selected decision.

The first results of the final resolution of the image did not show any variation, while the response times ranged from a non-significant second time to be considered. However, the difference is indicated in the structural similarity index. This value, being closer to one, corresponds to the fact that there is a greater structural similarity between the images evaluated. As the process is based on image restoration and reconstruction, this value must be the closest to one, while the signal-noise portion is the lowest. Noise can be corrected using filters. On the other

hand, the structural similarity index is more complex to correct since it changes the data matrix of the image. The use of bicubic interpolation was defined as a Super-resolution technique because it presented the best results for astronomical images.

2) *Focus filter*: When applied, the bicubic interpolation generates a blur of the image, which must be corrected to continue increasing the visual capabilities of the picture. A comparison was made between three non-pixel destructive motion correction filters: the Wiener filter, the Lucy-Richardson algorithm, and a regularized Gaussian filter.

As in the previous case, a low-resolution image captured by the system was selected, a movement of 2 mm to the right and 3 mm to the left per pixel was added to the image, which corresponds to an approximate of what generated in astronomical images by the rotation of the Earth. Subsequently, the response was evaluated by applying the selected filters.

The structural similarity index, the signal noise portion, the mean square error, and the processing time were evaluated in this process. As a first result, the Gaussian filter presented a high structural similarity. It was the one that took the least time because the Gaussian filter uses an auxiliary matrix with established parameters that are applied in a fixed way to the image without determining automatic correction parameters. This filter presented the optimal conditions, but it was defined to use the Wiener filter. It showed a slight improvement compared to the Gaussian filter and the lowest mean square error index. The Lucy-Richardson algorithm did not achieve the expected structural similarity indices, as it works best with high light brightness images, not astronomical images, so it was completely ruled out.

3) *Increase the contrast of the elements in the image*: For this process, it was defined to use a technique based on adding a percentage of the image's negative to enhance the elements found in the image. The inverse image of the image band is constructed: as the image scale is represented in grayscale, the black color corresponds to 0 and the white color to 255. Thus, the negative generates that the image elements are reflected of black color. Adding a percentage of the negative image allows enhancing the brightness of the elements in the image, making them more recognizable and managing to detect invisible elements within the image. The whole process is based on astrophotogrammetry techniques.

4) *Histogram equalizer*: This technique was chosen because it allows the histogram of an image to be distributed homogeneously by increasing its brightness and separating the slight variations between pixels of the image. Thus the picture is better visualized, and an increase in its quality is appreciated. The technique is used in astrophotography.

D. 4th Stage

By presenting the final result of the algorithm, a high-resolution image is delivered that is born from low-resolution images, which corresponds to the foundation of super-resolution.

E. Materials

A Raspberry Pi3 Model B + computer was used. It is a single-board computer developed in the UK by the Raspberry Pi Foundation. The board is focused on performing processes with few computational resources and is most used by atmospheric monitoring and control systems. Four Raspberry Pi V2 NOIR cameras were used, composed of an 8 megapixel Sony IMX219 sensor. The Image Processing Toolbox was used for algorithm development, a Matlab extension that provides a complete set of reference algorithms and workflow applications for image processing, analysis, visualization, and algorithm development. The Image Processing Toolbox performs image segmentation, image enhancement, noise reduction, geometric transformations, and image registration. In Fig. 3, the built All-Sky system is shown.

F. Operational Design

The operational design was established to define the optimal operating relationship of the algorithm. Table I indicates the conditions of the initial images for super-resolution.

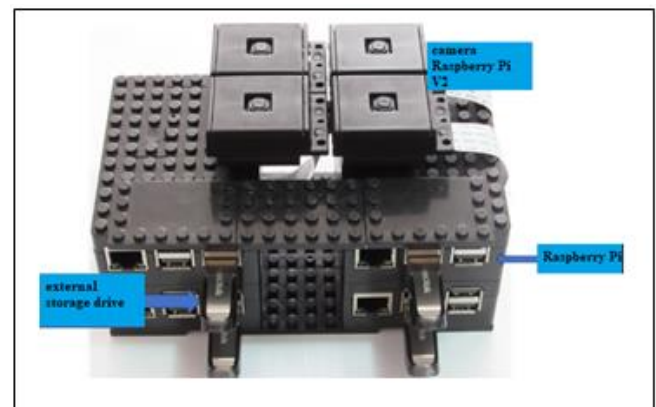


Fig. 3. System All-Sky.

TABLE I. SPECIFICATIONS FOR THE INITIAL IMAGES

Image type	Nightly
Picture format	RAW
Capture schedule	23:00 hrs until 05:00 hrs, this schedule is valid for both winter and summer
Number of images	4 images captured simultaneously by 4 different sensors
Exposition time	30000 ms to 60000 ms
Capture time between shots	Between 0.5 s to 1 s maximum
Maximum observation height	500 km limit of the atmosphere and outer space
Cloudiness	0% - 5%
Moon	0% to 30%
Brightness	10-21x to 10-31x
Humidity	0% to 10%

G. Algorithm Design

This task established the need for an algorithm that would allow four images captured simultaneously to obtain an image in super-resolution. The algorithm will work in the following sequence:

- Set 1: It consists of 4 atmospheric images.
- Process: The algorithm sequence follows a complete process. In this stage the subroutines for band separation, bicubic interpolation, Wiener filter, and element enhancement are performed.
- Solve: Delivers a result according to what is requested.
- Stores: The processed information is stored and accessible
- Set 2: Processed data folder

III. RESULTS

The evaluations carried out consisted of establishing a simulation model, based on different percentages of

resolutions of the images captured by the All-Sky system, to then compare them with images captured by a professional camera; This process consisted of establishing a comparison of the initial images with reference parameters, without reference and with printed graphics.

The final resolution of the algorithm was preset to each image separately so that it will reach 12 Mpx, since the exact resolution was needed to compare with an image captured by a Canon PowerShot SX510 HS professional camera.

Three image quality parameters defined in quality standards were evaluated: first, the mean square error (MSE), the signal-noise portion (PSNR), and the structural similarity index (SSIM).

Table II shows the results of the evaluations carried out on the parameters above, and in Fig. 4, the behavior of the quality parameters is graphically presented.

TABLE II. EVALUATION OF QUALITY PARAMETERS

N	Comparison results from the original image versus an image with SR				
	<i>Mpx Initial</i>	<i>Mpx Final</i>	<i>MSE</i>	<i>PSNR</i>	<i>SSIM</i>
1	0,08	12	220,7396	24,6920	0,6829
2	0,32	12	209,7571	24,9136	0,6877
3	0,73	12	201,4548	25,0890	0,6992
4	1,29	12	197,3120	25,1793	0,7010
5	2,02	12	195,6223	25,2166	0,7018
6	2,91	12	194,4457	25,2428	0,7023
7	3,96	12	193,0714	25,2736	0,7039
8	5,17	12	191,7464	25,3035	0,7059
9	6,55	12	190,4583	25,3351	0,7086
10	8,08	12	190,0195	25,3428	0,7107

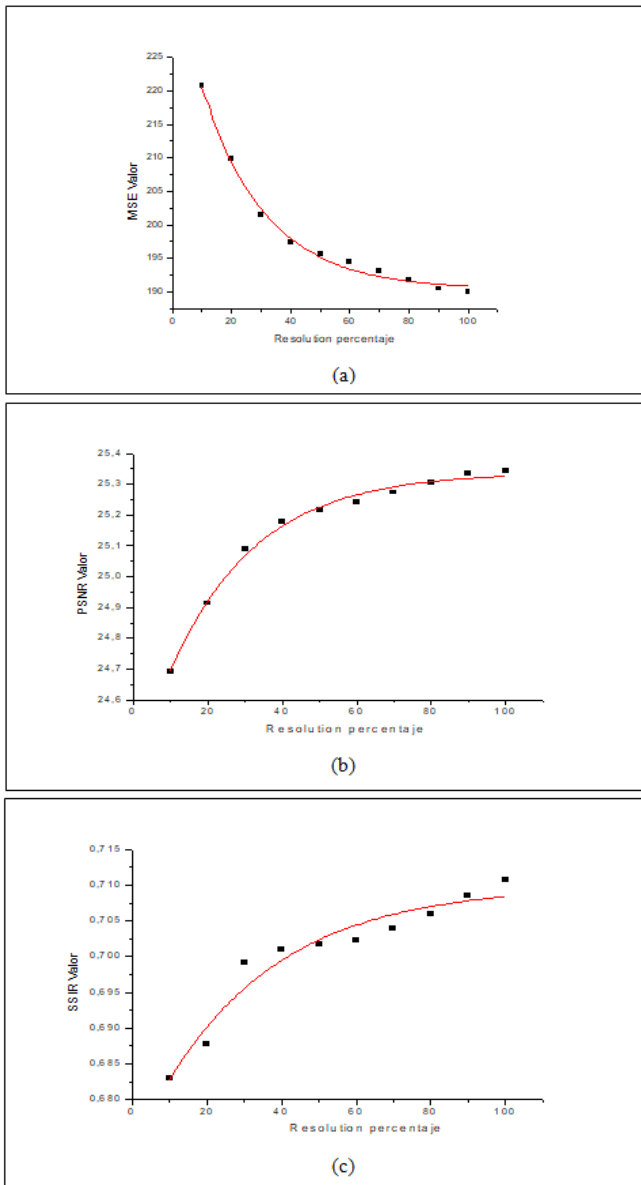


Fig. 4. Quality parameters, a) mean square error (MSE), b) the signal-noise portion (PSNR), and c) the structural similarity index (SSIM).

In Fig. 4a), it is noted that as the resolution of the images increases, the mean square error decreases. As the values fluctuate between 220 and 190, which are considered low, which measure the ratio of the pixels in the image, it was determined that the reconstruction of the image maintains a high degree of reliability. In Fig. 4b), it is noted that the signal-to-noise ratio decreases as the algorithm requires reconstructing a more significant segment for the image. In this case, the graph varies between 24 and 25, which are high values considered for this evaluation because these tests indicate the degree of distortion that the image presented. To affirm that the algorithm does not generate additive noise in its processes and restores the image with good results.

The structural similarity index is one of the most important parameters for these evaluations because it establishes whether the development of a super-resolution

algorithm based on the reconstruction and restoration of digital images is fulfilled. This process indicates the differences between the original image with the processed one according to its luminance, contrast, and structural information. According to the results obtained, it is indicated that these were favorable (Fig. 4c), since this value varied between 0.68 and 0.72, which suggests that the structural matrix of the image was not modified despite the significant increase in its resolution, as is the case of the smallest starting from 0.08 Mpx to reach 12 Mpx, therefore, the algorithm achieves a percentage of 70% structural stability in its processes.

The non-referenced quality parameters compare the statistical characteristics of the input image with a set of characteristics derived from a database of images generated from the original image. In Fig. 5, the behavior of these quality parameters are graphically presented.

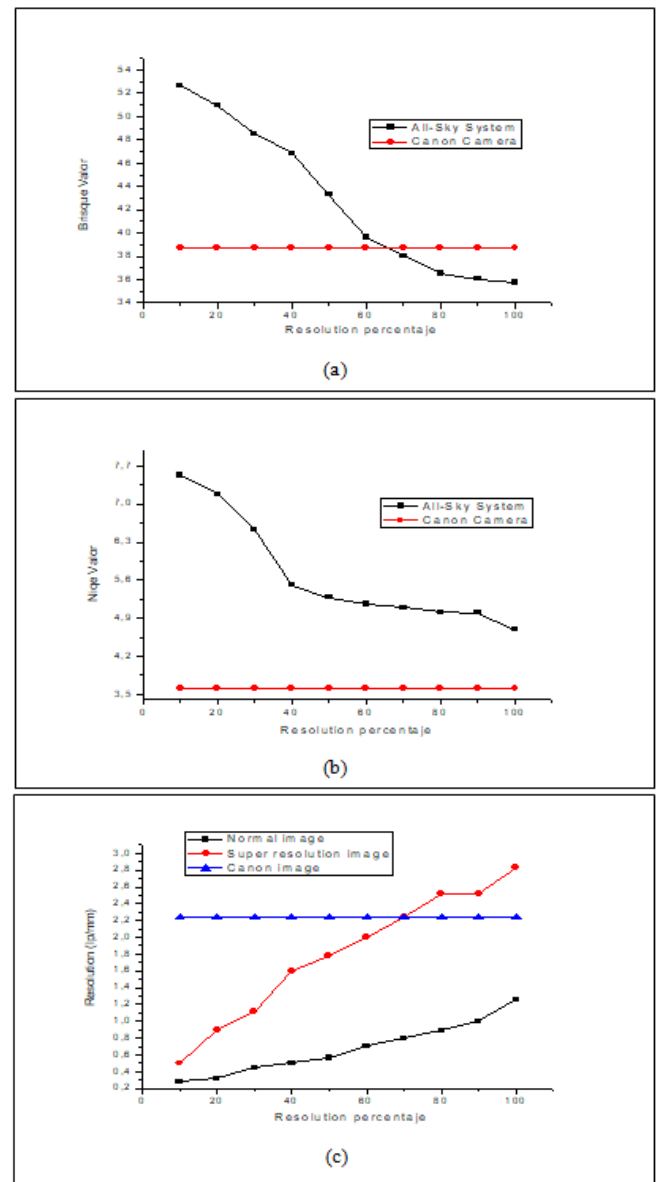


Fig. 5. Quality parameters, a) Brisque parameter, b) Niqe parameter and c) USAF Image Quality 1951 image quality parameter.

With the blind / non-referenced spatial quality parameter *Brisque*, the processed image and the image captured with a professional camera were evaluated, both with the same scenery. The Super-resolution images were adapted to the exact resolution as the professional image, and each image was captured individually with its assigned resolution according to the established percentage. In Fig. 5a) the results obtained from this parameter are presented, having the lowest value for the image that shows a better quality. The maximum resolution of the system processed with the algorithm obtains a lower score value than the image captured by a professional camera which means it is better. From this information, the same image as the digital camera can be reconstructed from a resolution of 70% of the sensor that corresponds to 3.96 Mpx (in the graph, the intersection point fits the resolution of 70%).

The *Niqe* naturalness image quality parameter determines the degree of manipulation that a digital image has suffered since its capture, manipulation generated from image processing models.

Fig. 5b) shows the comparison of this parameter between the All-Sky system and the Canon camera. The lower the resolution of the initial image, the greater the correction made by the algorithm to the final image. Therefore, this graph allows verifying that there is an image processing in the compared pictures. A degree of naturalness of the same similarity as the image of the professional camera cannot be obtained.

Finally, based on test graphics, the fineness or visible details in an image, it was evaluated with the quality parameter. The smaller the area represented by each pixel in a digital image, the greater the details reflected in the image. For this, the image quality model of the USAF Quality image was adapted, with a table of data measurements. In Fig. 6, the process of taking images and selecting stripes to evaluate image quality is shown.

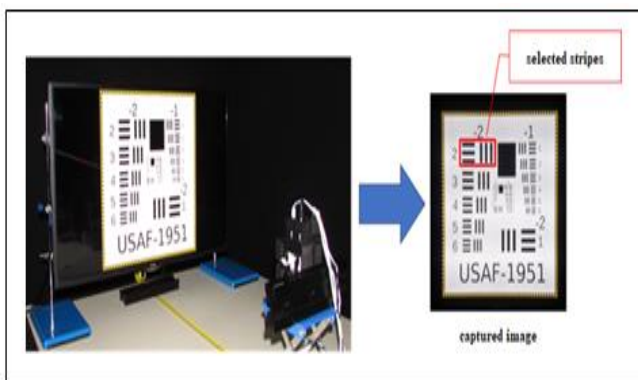


Fig. 6. Selection of USAF-1951 grid stripes

In this test, each segment of the image maintains a value associated with its position and resolution. When the stripes of the image preserve the same amount of pixel data, both vertical and horizontal, this group is selected to establish the resolution level. Each image was analyzed separately with its different resolutions and processed at the resolution of a professional camera. In Fig. 5c), comparing the data obtained with the initial or normal image captured by the system, the processed image and the image captured by the professional camera are shown. Here it can be identified that the image processed in Super-resolution reaches the exact resolution as the image captured by a professional camera at 70% of its resolution, which corresponds to a picture of 2296x1725 pixels, approximately 3.96 Mpx.

Finally, the test graphics made it possible to establish a real resolution value that the image processing algorithm achieves. These tests determined the correct image enhancement ratio from the resolutions obtained by the designed system and compared the image captured by a professional camera. The value corresponds to 126%, which is the percentage of improvement of the original and processed image resolutions. In Fig. 7, a low-resolution segment of an atmospheric image and the result of its processing are presented.

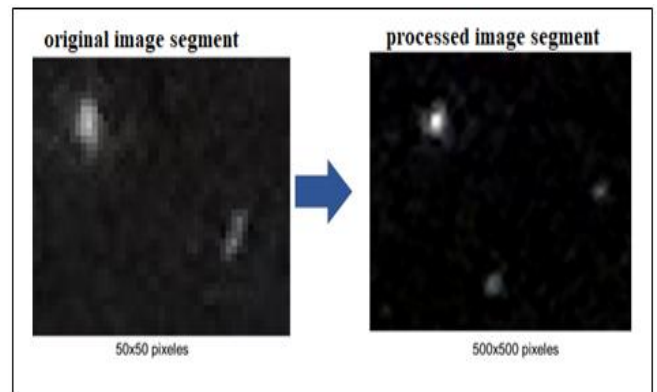


Fig. 7. Original image and processed with Super-resolution algorithm.

Fig. 8 shows a transient object captured by the camera system and using the Super-resolution algorithm. Finally, Fig. 9 shows another example of the result of the use of the super-resolution algorithm developed

IV. CONCLUSION

It is possible to establish that the algorithm achieves high reliability in its processes because the fluctuations of the results do not vary by more than 2% of the values given for both the MSE and PSNR. However, there is a loss of the structural matrix of the image because the similarity reaches only 70%, which indicates that the algorithm modifies the matrix by 30% to reconstruct the final image generated by the increased detail of the final image.

On the other hand, the quality metric values indicate that the image of a professional camera can be reconstructed with a resolution of 70%. This value could be determined since a comparison parameter of an image captured by a camera differs from that of the All-Sky system.

The test graphics made it possible to establish a real resolution value that the image processing algorithm achieves. These tests determined the correct image enhancement ratio from the resolutions obtained by the system and the comparison of the image captured by a professional camera. The value corresponds to 126%, which is the percentage of improvement of the resolutions made of the original and the processed image.

ACKNOWLEDGMENT

This material is based upon work supported by the Air Force Office of Scientific Research under award number FA9550-19-1-0028.

REFERENCES

- [1]. Sahar Ismail. "Super Resolution". Lambert. Pag 29-51. 2017
- [2]. C. Ledig, L. T. " Photo-Realistic Single Image Super-Resolution Using a Generative Adversarial". IEEE Xplore. 2018
- [3]. A. Shah. " Image Super Resolution-A Survey". Communication and Networking.2012
- [4]. Thomas Schildknecht. "Optical surveys for space debris". The Astronomy and Astrophysics Review, 14(1):41–111, 2007.
- [5]. Ryan Daniel Coder. "Multi-objective design of small telescopes and their application to space object characterization". PhD thesis, Georgia Institute of Technology, 2016.
- [6]. JM Trigo-Rodríguez, AJ Castro-Tirado, J Llorca, J Fabregat, VJ Martínez, V Reglero, M Jelínek, P Kubánek, T Mateo, and A de Ugarte Postigo. "The development of the spanish fireball network using a new all-sky ccd system". In Modern Meteor Science An Interdisciplinary View, pages 553–567. Springer, 2005.
- [7]. Peter Gural and Damir Segon. "A new meteor detection processing approach for observations collected by the croatian meteor network (cmn). WGN", Journal of the International Meteor Organization, 37:28–32, 2009.

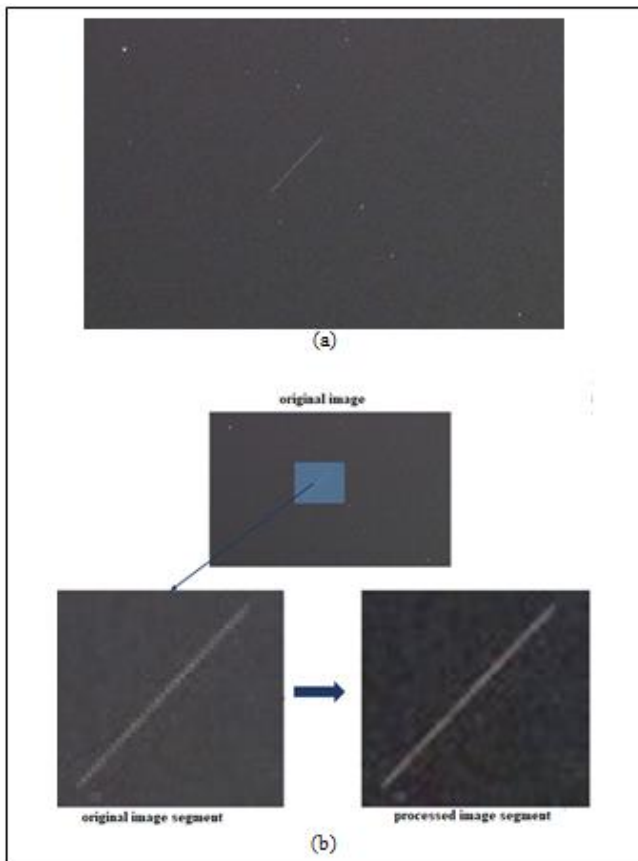


Fig. 8. a) Transient astronomical element detection and b) Transient element super-resolution.

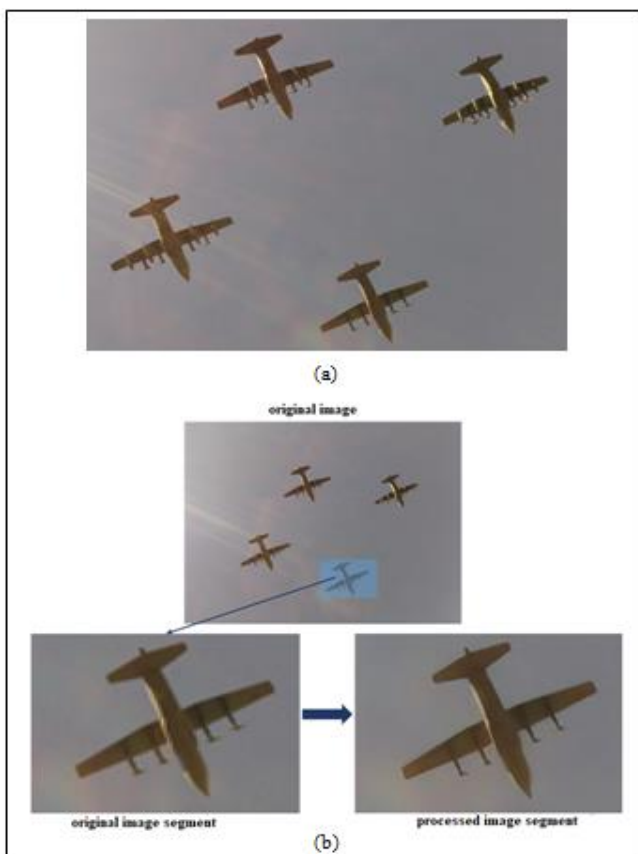


Fig. 9. a) Transient astronomical element detection and b) Transient element super-resolution.

- [8]. RJ Weryk, PG Brown, A Domokos, WN Edwards, Z Krzeminski, SH Nudds, and DL Welch. "The southern ontario all-sky meteor camera network". *Earth, Moon, and Planets*, 102(1-4):241–246, 2008.
- [9]. RJ Weryk, MD Campbell-Brown, PA Wiegert, PG Brown, Z Krzeminski, and R Musci. "The canadian automated meteor observatory (camo): system overview". *Icarus*, 225(1):614–622, 2013.
- [10]. J Jones, P Brown, KJ Ellis, AR Webster, M Campbell-Brown, Z Krzeminski, and RJ Weryk. "The canadian meteor orbit radar: system overview and preliminary results". *Planetary and Space Science*, 53(4):413–421, 2005.
- [11]. S Ríos Bergantiños, B Deguine, A Klotz, C Thiebaud, J Foliard, and M Boër. "Improvement of the tarot system used for space debris optical observations and observation campaign results". In *4th European Conference on Space Debris*, volume 587, page 125, 2005.
- [12]. Myrtille Laas-Bourez, Gwendoline Blanchet, Michel Boër, Etienne Ducrotté, and Alain Klotz. "A new algorithm for optical observations of space debris with the tarot telescopes". *Advances in Space Research*, 44(11):1270–1278, 2009.
- [13]. Michel Boër, Alain Klotz, Romain Laugier, Pascal Richard, Juan Carlos Dolado Pérez, Laurent Lapasset, Agnès Verzeni, Sébastien Théron, David Coward, and JA Kennewell. "Tarot: a network for space surveillance and tracking operations". In *7th European Conference on Space Debris ESA/ESOC, Darmstadt/Germany*, 2017.
- [14]. M Grøtze, S Virani, M Holzinger, A Register, C Perez, and J Tapia. "All-sky image fusion for a synoptic survey telescope in arctic and antarctic domains". In *Advanced Maui Optical and Space Surveillance Technologies Conference*, 2016.
- [15]. Peter S Gural. "Algorithms and software for meteor detection". *Earth, Moon, and Planets*, 102(1-4):269–275, 2008.
- [16]. Denis Vida and Filip Novoselnik. "Croatian meteor network: data reduction and analysis". In *Proceedings of the International Meteor Conference, Armagh, Northern Ireland*, pages 16–19, 2010.
- [17]. Denis Vida, Damir Šegon, Peter S Gural, Goran Martinovic, and Ivica Skokic. "Cmn_adapt and cmn_binviewer software". In *Proceedings of the International Meteor Conference, Giron, France*, pages 18–21, 2014.
- [18]. Filip Novoselnik, Ratko Grbic, and Dražen Sliškovic. "Image based meteor detection and path estimation". In *Smart Systems and Technologies (SST), International Conference on*, pages 307–312. IEEE, 2016.
- [19]. Myrtille Laas-Bourez, Gwendoline Blanchet, Michel Boër, Etienne Ducrotté, and Alain Klotz. "A new algorithm for optical observations of space debris with the tarot telescopes". *Advances in Space Research*, 44(11):1270–1278, 2009.
- [20]. P Zimmer, M Ackermann, and JT McGraw. "Gpu-accelerated faint streak detection for uncued surveillance of leo". In *Advanced Maui Optical and Space Surveillance Technologies Conference*, 2013.
- [21]. Peter Zimmer, John T McGraw, and Mark R Ackermann. Real-time surveillance of leo and meo with small optical telescopes.
- [22]. Timothy S Murphy, Marcus J Holzinger, and Brien Flewelling. "Space object detection in images using matched filter bank and bayesian update". *Journal of Guidance, Control, and Dynamics*, 40(3):497–509, 2016.
- [23]. Jenni Virtanen, Jonne Poikonen, Tero Sääntti, Tuomo Komulainen, Johanna Torppa, Mikael Granvik, Karri Muinonen, Hanna Pentikäinen, Julia Martikainen, Jyri Näränen, et al. "Streak detection and analysis pipeline for space-debris optical images". *Advances in Space Research*, 57(8):1607–1623, 2016.